

Spatiotemporal Magnonic Vortex Beams with Alternating Transverse Orbital Angular Momentum

Muyang Xie(谢沐阳)^{1*}, Chenchen Liu(刘晨晨)^{1*}, Jian Huang(黄剑)¹, Zhenyu Wang(王振宇)²,
Xinwei Dong(董新伟)¹, and Ruifang Wang(王瑞方)^{1**}

¹Department of Physics, Xiamen University, Xiamen 361005, China

²School of physics and electronics, Hunan University, Changsha 410082, China

*authors contributed equally to this work

**corresponding author. Email: wangrf@xmu.edu.cn

Recent theoretical and experimental studies revealed spatiotemporal photonic, and acoustic, vortex beams in open space. The spatiotemporal vortex beams carry orbital angular momentum perpendicular to the wave propagation direction. Here, we report spatiotemporal magnonic vortex beams in a confined geometry of a ferromagnetic nanostrip. The spatiotemporal magnonic vortex beam contains immobile phase dislocations and the wave propagates in a zigzag-like route. It is remarkable that the transverse orbital angular momentums, carried by the phase dislocations, are spatially alternating. Our findings are in sharp contrast to the photonic and acoustic counterparts, and open a new area in the study of spatiotemporal vortex beams.

Vortex beams carrying orbital angular momentum (OAM) is widely studied in photonics[1-5], acoustics[6,7], electronics[8-11] and magnonics[12-14]. The orientation of OAM is associated with the spatial structure of the phase front. For vortex beams with longitudinal OAM, there is a characteristic screw phase dislocation[15,16] aligned with the propagation axis and the wave amplitude is zero at the core. Its phase profile depends on the azimuthal angle φ in the form of $e^{il\varphi}$, in which l is an integer and denotes the topological charge of the vortex. The longitudinal OAM is collinear to the beam axis and has the quantized value of $l\hbar$. Experimental and theoretical studies[3,6,7,17] have demonstrated that the OAM exerts torque on microscopic particles. The value of OAM can be very large which provides new technological routes in information transmission[2,4,9,10].

More recently, spatiotemporal (ST) vortex beams with an edge, or mixture of edge and screw, phase dislocation were predicted theoretically[18-21] and observed experimentally in optics[22-25], and in acoustics[26,27]. Unlike the conventional vortex beam, which exist in 3D space or axis-symmetric medias, the ST vortex beams can propagate in 2D space. And the wave fields carry transverse OAM[3,20,24] that is orthogonal to the direction of propagation. In this letter, we report ST magnonic vortex beams in a ferromagnetic nanostrip with a vortex domain wall in the middle. After magnonic plane waves pass through the vortex domain wall, the spin-wave propagates along a “zigzag-like” path. The tilting of wave fronts is nonuniform in both spatial and temporal domains. Four phase singularities of edge, or mixture of edge and screw, type are observed. All the phase dislocations are stationary. And the transverse OAM oscillates spatially between \hbar and $-\hbar$.

We consider a ferromagnetic nanostrip in the x - y plane with its magnetization direction denoted by unit vector \mathbf{m} in Fig. 1(a). The magnetization dynamic of the nanostrip is governed by the Landau-Lifshitz-Gilbert (LLG) equation:

$$\frac{\partial \mathbf{m}}{\partial t} = -\gamma \mathbf{m} \times \mathbf{H}_{eff} + \alpha \mathbf{m} \times \frac{\partial \mathbf{m}}{\partial t}, \quad (1)$$

where γ and α are the gyromagnetic ratio and the Gilbert damping, respectively.

The sample is 2500 nm long, 202 nm wide and 5 nm thick. To study the magnetization dynamics, micromagnetic simulations are performed using the OOMMF code[28]. The material parameters of permalloy ($\text{Ni}_{0.8}\text{Fe}_{0.2}$) is used: magnetocrystalline anisotropy constant $k = 0 \text{ J/m}^3$, exchange coupling

constant $A = 1.3 \times 10^{-11}$ J/m, saturation magnetization $M_s = 8.0 \times 10^5$ A/m and the damping constant $\alpha = 0.01$. In the initial magnetization state, a stable tail-to-tail vortex domain wall locates in the middle of the nanostrip. The magnetization is nearly uniform and aligns with the $-\hat{e}_x$ (or $+\hat{e}_x$) direction on the left (or right) side of the wall. Inside the vortex domain wall, the magnetization curls clockwise (circularity $c = -1$) in the x-y plane, and the magnetization turns to the $+\hat{e}_z$ direction at the core (polarity $p = +1$), as illustrated in Figs 1(a) and 1(b). To reduce spin-wave reflection, the damping constant α gradually increases from 0.02 to 1.0 in the left and right end of the nanostrip. The triangular shape of the ends is designed to keep magnetization uniform in these regions.

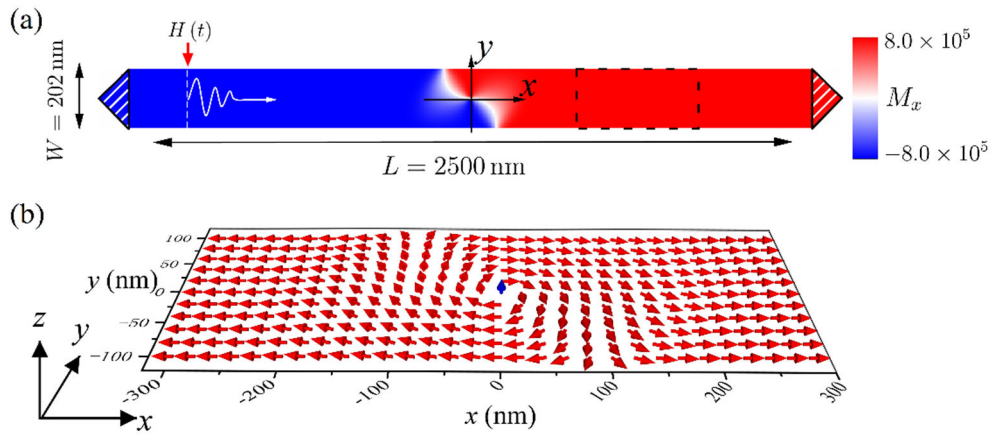


Fig. 1. Illustration of the initial magnetization state of the nanostrip. (a) A tail-to-tail vortex domain wall locates in the middle of the sample. The left and right ends, heightened as black triangles with white strips, of the nanostrip is designed to gradually shrink in width, in attention to reduce magnetic charge and maintain uniform magnetization. To minimize spin-wave reflection, higher damping constants varying from 0.02 to 1.0 are used in the left and right ends. The black dashed box indicates the area where FFT calculations are conducted. (b) Snapshot of the magnetization configuration of the vortex domain wall. The red arrows depict the magnetization direction. The vortex wall has clockwise magnetization circulation and upward polarity at the core.

The dynamical magnetization \mathbf{m} can be decomposed as $\mathbf{m} = \mathbf{m}_0 + \Delta\mathbf{m}$, where \mathbf{m}_0 is the static magnetization and $\Delta\mathbf{m}$ ($\ll \mathbf{m}_0$) is the spin-wave excitation part[29,30]. Apart from the

vortex domain wall, the static magnetization \mathbf{m}_0 is along $\pm\hat{\mathbf{e}}_x$, and the x -component of $\Delta\mathbf{m}$ is nearly zero. Therefore, the spin-wave excitation can be approximated as $\Delta\mathbf{m} = (0, \Delta m_y, \Delta m_z)$. Moreover, the $\hat{\mathbf{e}}_y$ orientation of excitation field leads to much larger Δm_y than Δm_z .

Previous studies show that plane waves passing through a 180 degree domain wall results in a phase shift of $\pi/2$ [31,32]. Side jump and skew scattering are reported for spin-waves across magnetic skyrmions and chiral domain walls[29,30]. So far, there is little study on the spin-wave modes after a magnonic plane wave passes through a magnetic texture with inhomogeneous magnetization.

To study the spin-wave modes in the nanostrip, a sinc-function field in the form of $\mathbf{B}_s = \hat{\mathbf{e}}_y B_s \sin[2\pi f(t - t_0)]/[2\pi f(t - t_0)]$, with $B_s = 50 \text{ mT}$, $f = 50 \text{ GHz}$ and $t_0 = 200 \text{ ps}$, is applied on a narrow region of $-950 \text{ nm} \leq x \leq -940 \text{ nm}$ for 10 ns. Fast Fourier transformation (FFT) on the average y -component of spin-wave excitation $\langle \Delta m_y \rangle$ is conducted in the area $350 \text{ nm} \leq x \leq 750 \text{ nm}$, i.e. after the spin-waves travel through the vortex domain wall, as illustrated in Fig. 1(a). In Fig. 2, the FFT amplitude spectrum shows spin-wave modes at frequencies of 4.7, 5.4, 6.6, 7.5, 9.2, 10.9 and 11.5 GHz. The spatial distribution of these modes is displayed by Figs S1 and S2 in supplemental data. The first four modes are common plane waves, while the mode with $f = 9.2 \text{ GHz}$ clearly demonstrates twisted wave fronts rotating in the x - y plane. The modes at 10.9 and 11.5 GHz are similar, but have more complicated phase structures.

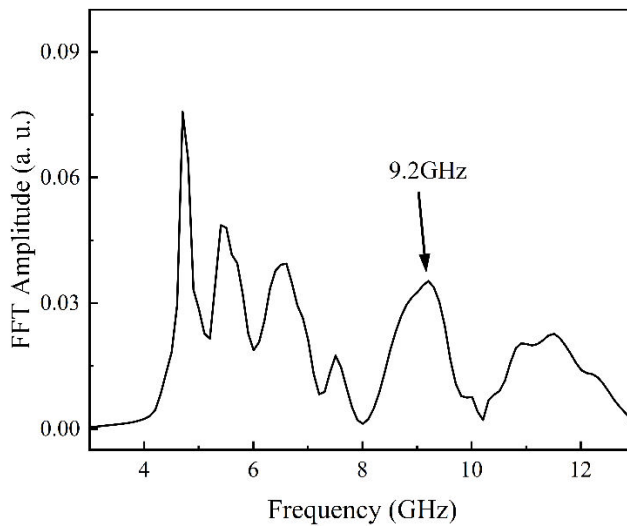


Fig. 2. FFT spectrum of the spin-waves passing through the vortex domain wall. The spectrum shows a few spin-wave modes. The 9.2 GHz mode is identified as a ST magnonic

mode and is studied in detail in this work.

To study the continuous spin-wave propagation, a sinusoidal field of the form $\vec{B}(t) = \hat{e}_y B \sin 2\pi f t$, with $f = 9.2$ GHz and $B = 50$ mT, is applied on the area between -950 nm $\leq x \leq -940$ nm for 10 ns. The excitation field stimulates spin-waves with parallel wave fronts, i.e., plane waves, until they are scattered by the vortex domain wall, as shown in Fig. 3. By defining local spherical coordinates $(\hat{e}_r, \hat{e}_\theta, \hat{e}_\varphi)$ and letting $\hat{e}_r = \mathbf{m}_0$, the spin-wave excitation can be expressed as[29] $\Delta\mathbf{m} = \Delta m_\theta \hat{e}_\theta + \Delta m_\varphi \hat{e}_\varphi$, or as a complex field $\psi(\mathbf{r}, t) = \Delta m_\theta - i\Delta m_\varphi$. The spin-wave flux[29] is then defined as $\mathbf{j} = -iA(\psi^* \nabla \psi - \psi \nabla \psi^*)/2$. Before the magnonic plane wave encounters the vortex domain wall, it travels straightly along \hat{e}_x direction, and the intensity of flux ($|\mathbf{j}|$) distributes symmetrically across the width of the nanostrip, where the maximum intensity is found in the middle ($y = 0$). The inhomogeneous magnetization texture of vortex domain wall results in splitting of spin-wave flux. Much more flux is scattered to the upper half of the nanostrip than to the lower half. Flux singularities are observed at both the core of vortex domain wall and other locations in the vicinity, as shown in Fig. 3.

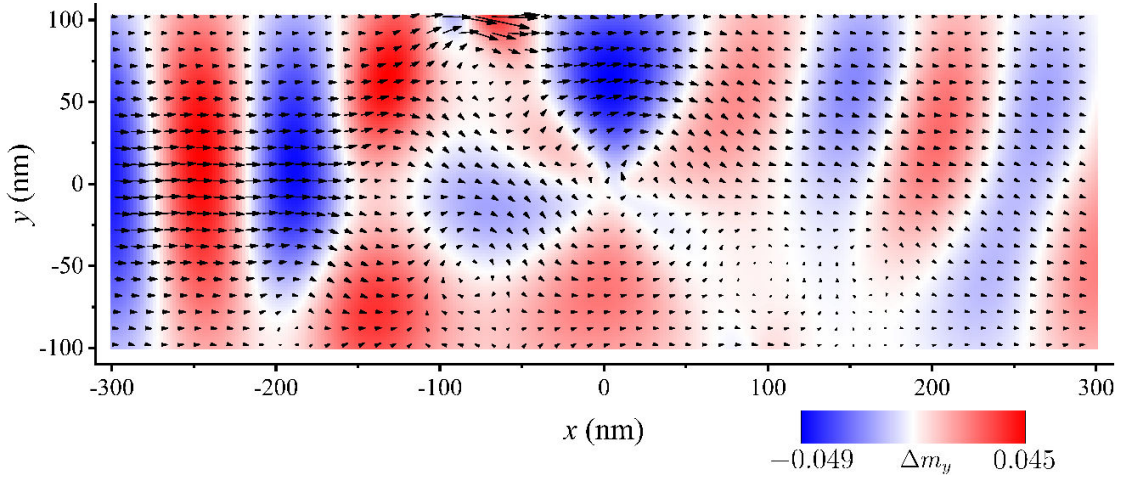


Fig. 3. Spin-wave scattering by the vortex domain wall. The background color illustrates the spatial variation of Δm_y . Black arrows correspond to the local spin-wave flux \mathbf{j} . The length of the arrows is proportional to the flux intensity.

After the spin-wave passes through the domain wall region, it propagates along a zigzag-like path as shown in Fig. 4(a), in sharp contrast to not only the spiral route of vortex beams, but also the

straight path of ST optical[22-24], and acoustic[26], beams in open space. Meanwhile, the spatial distribution of Δm_y is in accordance with the zigzag-like flux path. The strongest spin-wave flux is found at where the spin-wave excitation is highest. Flux vortices are observed as well. Flux singularity and null spin-wave excitation are found at the vortex cores. For the four flux vortices from left to right in Fig. 4(a), their circularity c changes regularly as -1 , $+1$, -1 and $+1$, respectively. In this way, the topology of vortices is compatible with the flux of spin-wave.

Figure 4(b) demonstrates periodical tilting of phase fronts, a characteristic topology for waves carrying OAM. The wave fronts rotate around z -axis, while the wave propagates in the x - y plane. The rotation of wave fronts is both spatially and temporally non-uniform. This leads to phase dislocations of edge type, or mixture of edge and screw type, as shown in Fig. 4(b).

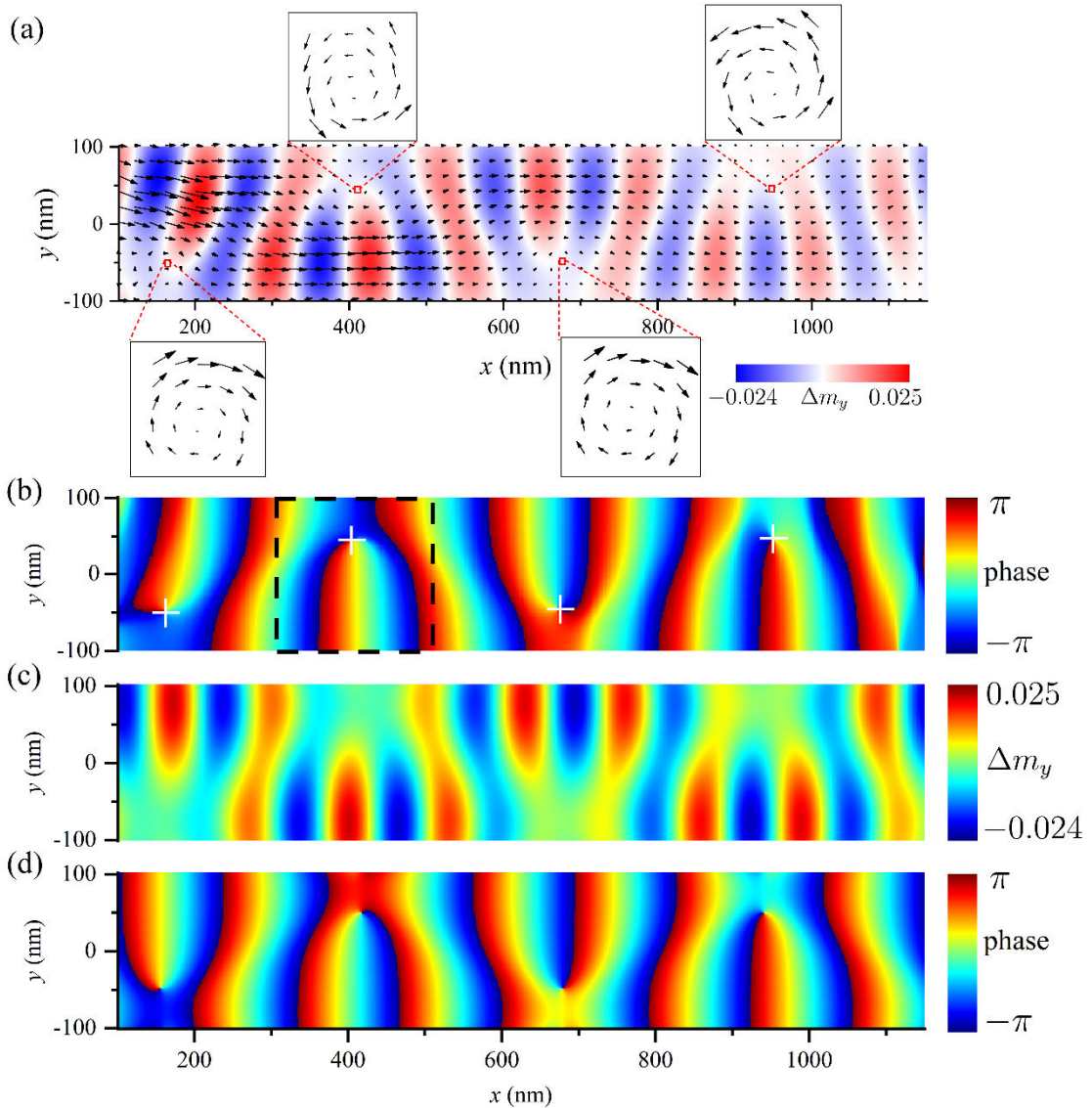


Fig. 4. Snapshots of the spin-wave after passing through the vortex domain wall. The plots correspond to the instant time at $t = 5000$ ps, while $t = 0$ corresponds to onset of the excitation field. In (a), the background color illustrates the micromagnetic simulation result of spatial variation of Δm_y . The spin-wave flux \mathbf{j} is denoted by black arrows. The distribution of spin-wave excitation Δm_y is in accordance with the zigzag-like path of spin-wave flux. (b) Micromagnetic simulation result of phase distribution of the ST spin-wave excitation Δm_y . The tilting wave fronts create four phase singularities marked with white crosses. The phase singularities are of either edge or mixture of edge and screw type. Theoretical results, using equation (3), of the distribution of Δm_y and corresponding phase are displayed in (c) and (d), respectively.

The OAM carried by the spin-wave can be calculated[17] as

$$\mathbf{L} = \frac{\hbar}{S} \iint (\nabla\phi \times \mathbf{r}) dx dy, \quad (2)$$

where $\phi = \arg(\Delta m_y + i\Delta m_z)$, \mathbf{r} is measured relative to the phase singularity and S is a small area surrounding the singularity, as shown in Fig. 5. Because both $\nabla\phi$ and \mathbf{r} are in the x - y plane, \mathbf{L} is perpendicular to the x - y plane, i.e. the OAM is transverse in nature. Substituting the spin-wave excitation Δm_y and Δm_z into (2) and letting S be a circle of radius 50 nm, we obtain $L = -\hbar$, $+\hbar$, $-\hbar$, $+\hbar$ for the four phase singularities from left to right, respectively. Note that, at each phase vortex, the sign of transverse OAM and the circularity of spin-wave flux is always the same. It is interesting that the OAMs vary periodically in both x and y dimension. Temporal evolution of one phase dislocation, marked by a dashed black box in Fig. 4(b), is demonstrated in Fig. 6. Similar effect, called “temporal diffraction”, was previously reported in ST photonic and acoustic waves[18,20,24,26]. It is seen that the structure of the phase dislocation undergoes a periodical change in $T = 110$ ps, i.e. the period of a 9.2 GHz wave. It is remarkable that all phase dislocations remain stationary, while the wave propagates in the nanostrip. In contrast, phase dislocations in ST optical, and acoustic, beams move along with the wave[20,26,27]. The difference may be attributed to the confined geometry in our study.

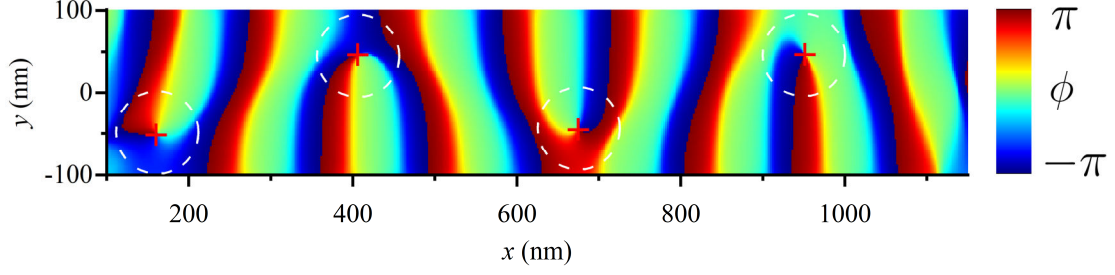


Fig. 5. The spatial distribution of $\phi = \arg(\Delta m_y + i\Delta m_z)$. Four phase vortices are marked with red cross. White dashed circle denotes the integration area to calculate the OAM, using equation (2).

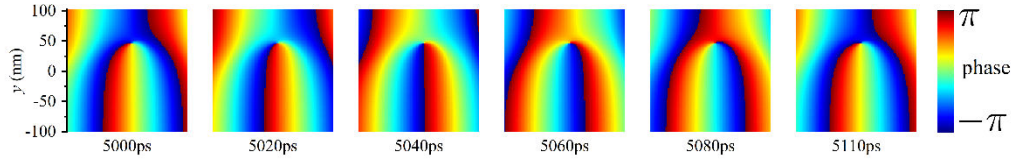


Fig. 6. Temporal variation of the phase dislocation enclosed by a dashed black box in Fig. 4(b). The structure variation undergoes a complete cycle in a period of 110 ps.

To explain the formation of ST vortex pulses in open space, Bliokh et al. [18,20,21] constructed Bessel-type solutions of scalar waves, using a superposition of plane waves with wave vectors distributed over a circle. Since the plane wave frequency depends on its wave factor, ST vortex pulses constructed by this way is polychromatic. And the phase dislocations travel with the beam. In this work, however, the vector spin-wave propagates in confined geometry of a nanostrip, while the phase dislocations are immobile. According to spatial FFT analysis displayed in Fig. S3 in supplemental data, the ST magnonic vortex beam is composed of three plane waves with discrete wave vectors. The evolution of Δm_y is expressed as:

$$\Delta m_y(x, y, t) = \text{Re}[Ae^{i(k_{x1}x - \omega t)} + Be^{i(k_{x2}x - k_y y + \frac{\pi}{2} - \omega t)} + Be^{i(k_{x2}x + k_y y - \frac{\pi}{2} - \omega t)}], \quad (3)$$

in which $k_{x1} = 5.4 \times 10^7 \text{m}^{-1}$, $k_{x2} = 4.2 \times 10^7 \text{m}^{-1}$, $k_y = 2.0 \times 10^7 \text{m}^{-1}$, $\omega = 2\pi \times 9.2 \text{GHz}$, and $A:B = 1.66$. We assume that the plane wave components have same frequency of 9.2 GHz. Otherwise, stationary phase dislocations cannot be obtained. Using equation (3), the theoretical distribution of Δm_y and corresponding phase at $t = 5000 \text{ps}$ is illustrated in Figs. 4(c) and 4(d) respectively, which are in good agreement with the simulation results in Figs. 4(a) and 4(b).

In conclusion, we revealed ST magnonic vortex beams in a ferromagnetic nanostrip, by means of passing planar spin-waves through a vortex domain wall. It is found that the ST spin-wave flux travels along an unusual zigzag-like route. The phase singularities are stationary, regardless of the wave propagation along the strip. Transverse OAMs associated with the phase dislocations evolve periodically in both the x and y dimension. The structure of phase dislocations shows periodical evolution in time, a clear demonstration of “temporal diffraction” of the ST magnonic vortex beam. Our results are in sharp contrast to previous studies on ST photonic (and acoustic) vortex beams in open space. Other than vortex domain walls, the low dimensional ferromagnetic systems are rich in magnetic textures[33], such as magnetic skyrmions, vortices, Bloch points, antivortices and merons. Therefore, we expect encouraging future for exploring new physics of ST magnonic vortex waves.

We acknowledge financial support by the National Natural Science Foundation of China under Grant No. 11174238.

- [1] M. Padgett, J. Courtial, and L. Allen, *Physics Today* **57**, 35 (2004).
- [2] L. Allen, M. W. Beijersbergen, R. J. C. Spreeuw, and J. P. Woerdman, *Phys. Rev. A* **45**, 8185 (1992).
- [3] K. Bliokh and F. Nori, *Physics Reports-Review Section of Physics Letters* **592**, 1 (2015).
- [4] A. Yao and M. Padgett, *Adv. Opt. Photon.* **3**, 161 (2011).
- [5] J. Harris, V. Grillo, E. Mafakheri, G. Gazzadi, S. Frabboni, R. Boyd, and E. Karimi, *Nature Physics* **11**, 629 (2015).
- [6] L. Zhang and P. Marston, *PhRvE* **84**, 065601 (2011).
- [7] C. Demore, Z. Yang, A. Volovick, S. Cochran, M. MacDonald, and G. Spalding, *Physical Review Letters* **108**, 194301 (2012).
- [8] G. Vanacore *et al.*, *Nat. Mater.* **18**, 573 (2019).
- [9] J. Verbeeck, H. Tian, and P. Schattschneider, *Nature* **467**, 301 (2010).
- [10] M. Uchida and A. Tonomura, *Nature* **464**, 737 (2010).
- [11] V. Grillo, G. Gazzadi, E. Mafakheri, S. Frabboni, E. Karimi, and R. Boyd, *Physical Review Letters* **114**, 034801 (2015).
- [12] C. Jia, D. Ma, A. F. Schaeffer, and J. Berakdar, *Nat. Commun.* **10**, 2077 (2019).
- [13] Y. Jiang, H. Y. Yuan, Z. X. Li, T. Wang, H. W. Zhang, Y. Cao, and P. Yan, *Physical Review Letters* **124**, 217204 (2020).
- [14] S. Lee and S. Kim, *FrPhy* **10**, 858614 (2022).
- [15] V. Bazhenov, M. Soskin, and M. Vasnetsov, *JMOp* **39**, 985 (1992).
- [16] V. Bazhenov, M. Vasnetsov, and M. Soskin, *Jetp Letters* **52**, 429 (1990).
- [17] Y. Jiang, H. Yuan, Z. Li, H. Wang, H. Zhang, Y. Cao, and P. Yan, *Physical Review Letters* **124**, 217204 (2020).
- [18] K. Bliokh and F. Nori, *Phys. Rev. A* **86**, 033824 (2012).
- [19] A. Sukhorukov and V. Yangirova, *Spatio-temporal vortices: properties, generation and*

- recording* (SPIE, 2005), Vol. 5949, Congress on Optics and Optoelectronics, p. pp. EOO.
- [20] K. Bliokh, Physical Review Letters **126**, 243601 (2021).
- [21] K. Bliokh, Phys. Rev. A **107**, L031501 (2023).
- [22] N. Jhajj, I. Larkin, E. Rosenthal, S. Zahedpour, J. Wahlstrand, and H. Milchberg, Phys. Rev. X **6**, 031037 (2016).
- [23] A. Chong, C. Wan, J. Chen, and Q. Zhan, Nature Photonics **14**, 350 (2020).
- [24] S. Hancock, S. Zahedpour, A. Goffin, and H. Milchberg, Optica **6**, 1547 (2019).
- [25] S. Hancock, S. Zahedpour, and H. Milchberg, Physical Review Letters **127**, 193901 (2021).
- [26] H. Ge, S. Liu, X. Xu, Z. Long, Y. Tian, X. Liu, M. Lu, and Y. Chen, Physical Review Letters **131**, 014001 (2023).
- [27] S. Liu, H. Ge, X. Xu, Y. Sun, X. Liu, M. Lu, and Y. Chen, Nat. Commun. **16**, 2823 (2025).
- [28] O. U. s. G. V. N. I. o. S. a. T. M. J. Donahue and D. G. Porter (1999), Gaithersburg, MD, 1999), <http://math.nist.gov/oommf/>.
- [29] J. Lan and J. Xiao, Physical Review B **103**, 054428 (2021).
- [30] H. Wu and J. Lan, Physical Review B **112**, 064410 (2025).
- [31] R. Hertel, W. Wulfhekel, and J. Kirschner, Physical Review Letters **93**, 257202 (2004).
- [32] C. Bayer, H. Schultheiss, B. Hillebrands, and R. L. Stamps, IEEE Transactions on Magnetics **41**, 3094 (2005).
- [33] H. Yu, J. Xiao, and H. Schultheiss, Physics Reports-Review Section of Physics Letters **905**, 1 (2021).

Supplemental Material

Spatiotemporal Magnonic Vortex Beams with Alternating Transverse Orbital Angular Momentum

Muyang Xie(谢沐阳)^{1*}, Chenchen Liu(刘晨晨)^{1*}, Jian Huang(黄剑)¹, Zhenyu Wang(王振宇)²,
Xinwei Dong(董新伟)¹, and Ruifang Wang(王瑞方)^{1**}

¹Department of Physics, Xiamen University, Xiamen 361005, China

²School of physics and electronics, Hunan University, Changsha 410082, China

*authors contributed equally to this work

**corresponding author. Email: wangrf@xmu.edu.cn

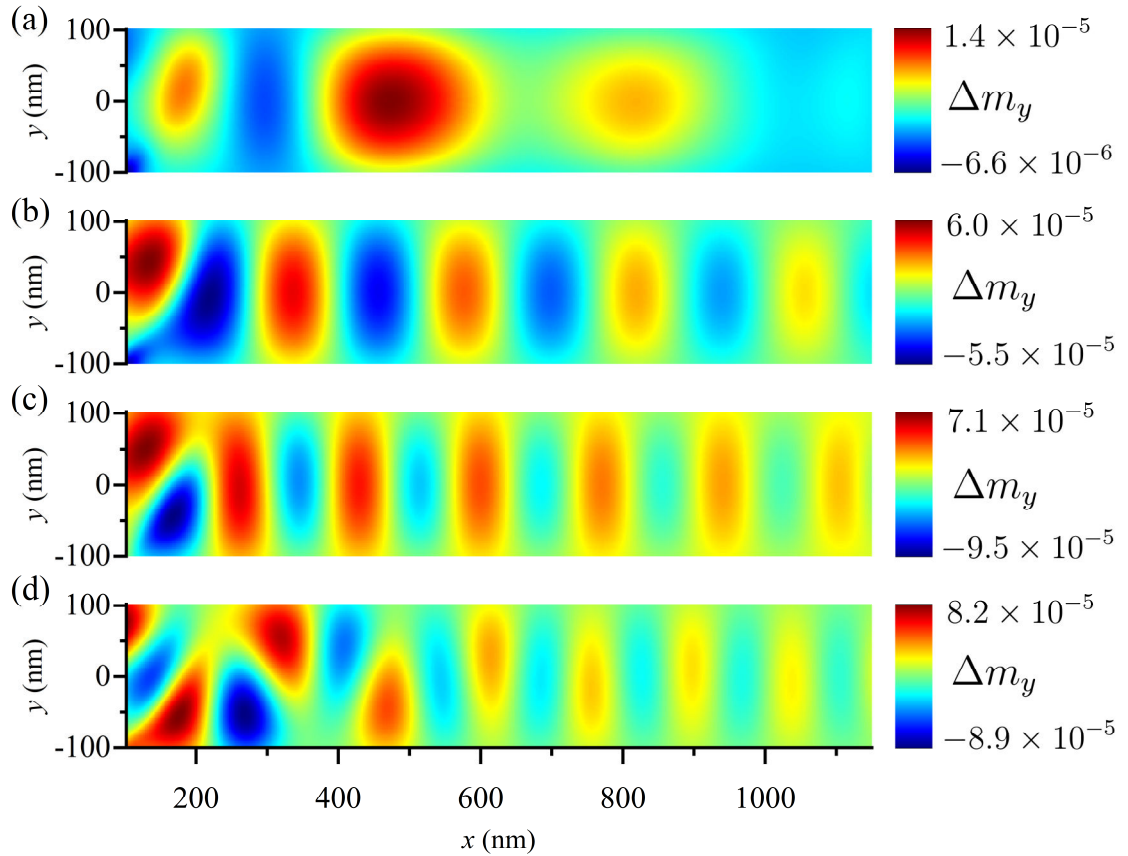


Fig. S1. Spatial variation of Δm_y for the spin-wave modes at (a) 4.7 GHz, (b) 5.4 GHz, (c) 6.6 GHz, and (d) 7.5 GHz, respectively. Parallel wave fronts indicate that these modes are conventional plane waves.

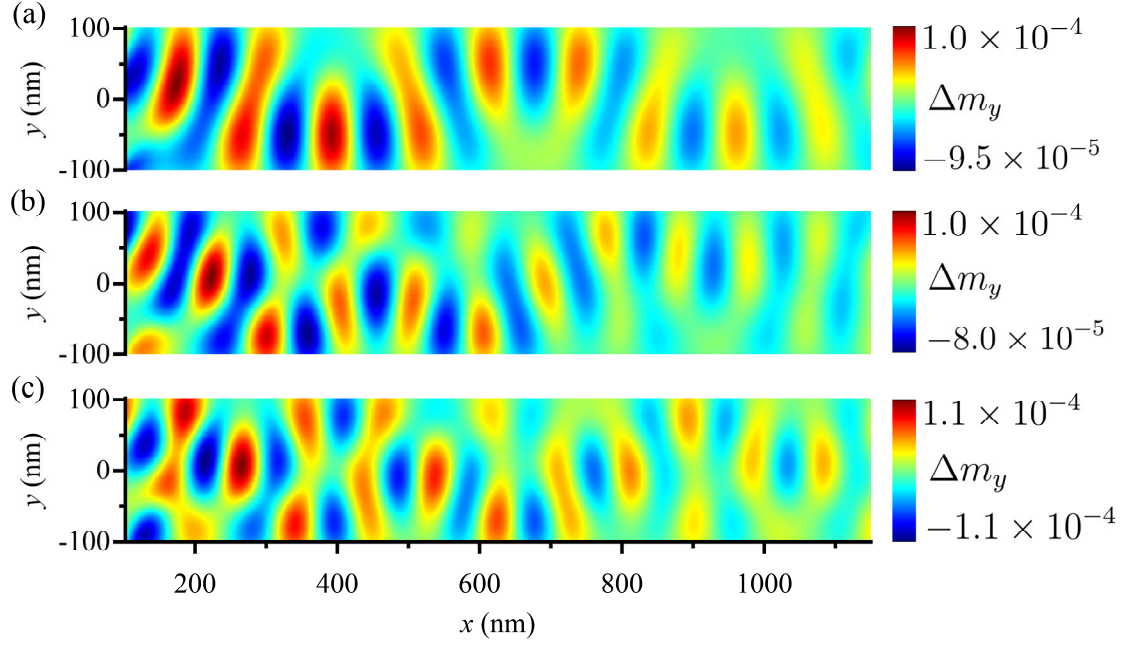


Fig. S2. Spatial variation of Δm_y for the spin-wave modes at (a) 9.2 GHz, (b) 10.9 GHz, and (c) 11.5 GHz, respectively. The wave fronts tilt in the x - y plane, indicating that these modes carry transverse orbital angular momentum.

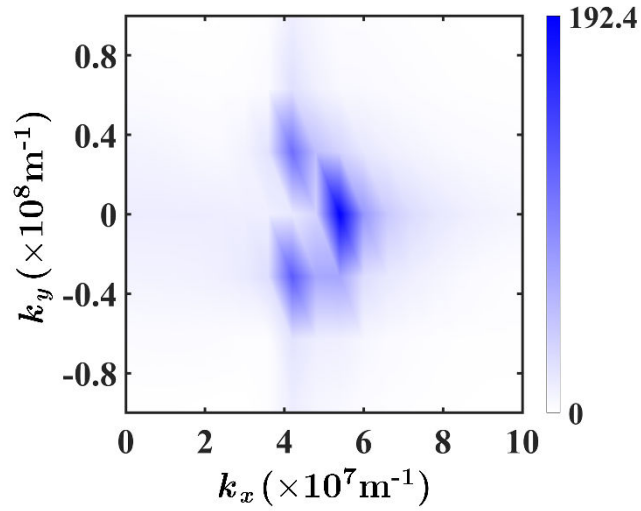


Fig. S3. Plane-wave spectrum of the ST magnonic vortex wave obtained by spatial FFT analysis. Intensity and wave vector of the three plane-wave components are used in equation (3) of the main text.